Chemical Science

ROYAL SOCIETY OF CHEMISTRY

EDGE ARTICLE

View Article Online
View Journal | View Issue

Cite this: *Chem. Sci.*, 2025, **16**, 7294

All publication charges for this article have been paid for by the Royal Society of Chemistry

Pd(μ-L)$_4$Pt *vs.* Pd(μ-L)$_4$RuCl$_2$: chlorido ancillary ligands as defining factors in the host–guest interactions of M(μ-L)$_4$M′ heterodimetallic supramolecular architectures†

Hayden B. Gearing, [a] Monika Cziferszky, [b] Tilo Söhnel, [ac] L. James Wright, [a] James D. Crowley *[cd] and Christian G. Hartinger *[a]

In supramolecular architectures, the interactions between host and guest molecules are governed by non-covalent forces such as hydrogen (H) bonding, hydrophobic and electrostatic interactions. We alter here the cavity microenvironment to control the interactions between guest and host molecules and study the effects of introducing axial chlorido ligands through the use of an octahedral building block in M(μ-L)$_4$M′ architectures. We prepared the heterodimetallic Pd(μ-L)$_4$Pt C^4_{Pt} and Pd(μ-L)$_4$RuCl$_2$ C^4_{Ru} architectures and demonstrated the role of 'classic' non-covalent forces in their host–guest chemistry with anionic and neutral molecules, while the cages also underwent disassembly and reassembly upon addition of external stimuli. This culminated in the isolation of a 1 : 1 host–guest complex between C^4_{Pt} and the dianionic 1,5-naphthalenedisulfonate which was characterized by single crystal X-ray diffraction studies. These showed the guest occupied the central cavity and was held in place by H bonding. The *endo*-chlorido ligand in C^4_{Ru} played an important role in the capture of neutral guest molecules. In particular, it allowed for finetuning of the cavity properties of the supramolecular architectures by limiting the formation of H bonds and restricting the cavity size while offering alternative interactions.

Received 9th January 2025
Accepted 21st March 2025

DOI: 10.1039/d5sc00209e

rsc.li/chemical-science

Introduction

In recent decades, self-assembled metallosupramolecular architectures (MSAs), such as M_2L_4-type cages, have been designed and studied for a wide range of applications.[1–5] For example, $[Pd_2L_4]^{4+}$ (or $[Pd(\mu\text{-}L)_4Pd]^{4+}$) MSAs have been examined for their use as catalysts,[6–8] as luminescent materials,[9,10] in medical applications,[11,12] for molecular recognition and, of particular interest, for their ability to encapsulate drugs and other molecules in host–guest chemistry.[5,13–15] In most cases for these cage-like hosts, binding of guest molecules is facilitated by non-covalent forces such as hydrogen (H) bonding, hydrophobic and coulombic interactions.[16–19]

The synthetic principles that direct the construction of high-symmetry architectures are well-understood.[3,20] These same strategies have also been used to great effect in installing secondary metal centers, which serve as structural and/or behavioral components.[21–26] However, recently lower-symmetry MSAs have been attractive targets as they may facilitate the introduction of different chemical properties into a single cage molecule. To this end many heteroditopic ligand scaffolds have been employed to generate lower symmetry architectures such as heteroleptic,[27–31] pseudo-heteroleptic,[32–34] and multi-cavity Pd(II)-based architectures.[18,29,35–39]

Another strategy, however, is to introduce non-symmetry by installation of different metal centers at either end of cage architectures to yield, for example, heterodimetallic MM′L$_4$ compounds. Such a strategy has been implemented to incorporate metal centers such as Fe,[40] Cu,[41] Ru,[42] Pt[43–46] and others, into [PdML$_4$] systems. The first syntheses of heterodimetallic [Pd(μ-L)$_4$Pt] cages were reported by Lisboa *et al.* using subcomponent self-assembly.[43] In a different approach, Pearcy *et al.* established a stepwise approach by sequential coordination of initially the more kinetically inert Pt(II) center followed by the more labile Pd(II) center to heterotopic imidazole and pyridyl *N*-donor scaffolds.[46] Preston and co-workers recently

[a]*School of Chemical Sciences, University of Auckland, Private Bag 92019, Auckland 1142, New Zealand. E-mail: c.hartinger@auckland.ac.nz*

[b]*Institute of Pharmacy/Pharmaceutical Chemistry, University of Innsbruck, Centre for Chemistry and Biomedicine, Innrain 80–82/IV, 6020 Innsbruck, Austria*

[c]*MacDiarmid Institute for Advanced Materials and Nanotechnology, Victoria University of Wellington, PO Box 600, Wellington 6140, New Zealand*

[d]*Department of Chemistry, University of Otago, PO Box 56, Dunedin 9054, NewZealand. E-mail: jcrowley@chemistry.otago.ac.nz*

† Electronic supplementary information (ESI) available: The syntheses of the MSAs, characterization data, additional figures of the molecular structures, experimental data for the disassembly and reassembly reactions, as well as host guest binding studies by NMR, ESI-MS and molecular modelling. CCDC 2389021–2389023. For ESI and crystallographic data in CIF or other electronic format see DOI: https://doi.org/10.1039/d5sc00209e

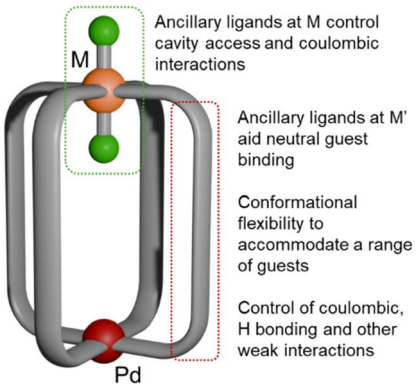

Fig. 1 Schematic structure of Pd(μ-L)$_4$RuCl$_2$ cages. Pd(II), red; Ru(II), orange; Cl, green; bridging ligand, grey.

introduced an alternative Pt-based building block for the construction of kinetically robust Pt_2L_4 cages.[47] In such MSAs, the different coordination properties of two metal centers or of different coordination motifs in ditopic ligands can be exploited for stimulus-induced partial (and reversible) disassembly of the host molecule, and release of a molecular guest.[17,40,43] For example, a $[Pd(\mu\text{-}L)_4Pt]^{4+}$ cage was found to bind benzoquinone and 2,6-diaminoanthraquinone guests strongly,[43] and also showed interactions with cisplatin and 5-fluorouracil. Only a few other examples of such MSAs have been reported since.[44,46–49]

Based on a preliminary study, in which we explored the preparation and sulfonate binding ability of $[Pd(\mu\text{-}L)_4Pt]^{4+}$ in comparison to cages featuring an octahedral *trans*-Ru(II)Cl$_2$ moiety in place of the Pt center ($[Pd(\mu\text{-}L)_4RuCl_2]^{2+}$; Fig. 1), we develop here a broad understanding of how the introduction of such a moiety to the cavity affects the guest binding properties of heterodimetallic architectures. Furthermore, we assessed the stimulus-responsive abilities of these cages for disassembly and reassembly, and the effect on binding of anionic guests.

Results and discussion

Making use of a modular approach in the subcomponent self-assembly of heterobimetallic MSAs,[43,44,46–49] we aimed to introduce rational changes to PdML$_4$ MSAs by altering the Pd···M distances through variation of the bridging ligands, exploring the impact of ancillary Cl ligands on M and the effects of coulombic, H bonding and hydrophobic interactions. We previously reported Pd(μ-L)$_4$RuCl$_2$ MSAs $\mathbf{C^1_{Ru}}$–$\mathbf{C^3_{Ru}}$ (Fig. 2) that allowed discrimination between small, similarly sized, anionic guest molecules by restricting the cavity size with axially-coordinated ligands to the Ru center while maintaining the stimulus-responsive reversible opening and closing of PdPt analogs.[49]

Extension of the Pd···M distances compared to previously reported heterodimetallic MSAs $\mathbf{C^1_{Pt}}$–$\mathbf{C^3_{Pt}}$ and $\mathbf{C^1_{Ru}}$–$\mathbf{C^3_{Ru}}$, and therefore enlargement of the cage cavity, was achieved by non-symmetric functionalization of 4,4′-methylenedianiline (MDA). MDA has been used to generate homometallic MSA with large

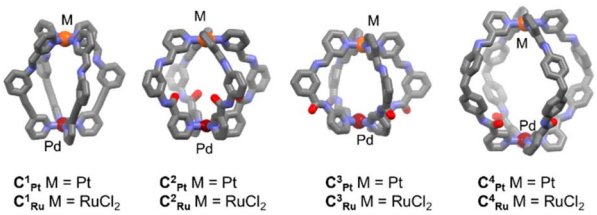

Fig. 2 Model structures for the systematic variation of Pd(μ-L)$_4$M MSAs $\mathbf{C^1_{Pt}}$–$\mathbf{C^4_{Pt}}$ and $\mathbf{C^1_{Ru}}$–$\mathbf{C^4_{Ru}}$ which feature different functionalities to control guest binding. M = Pt or RuCl$_2$.

accessible cavities.[50,51] While the MDA unit can undergo hydrophobic interactions with guest molecules to accommodate a wider array of guests, we introduced an amide motif at the Pd end of the cage instead of the alkynyl linker that was used previously.[49] The amide function can in principle act as either an H bond donor or acceptor. The second metal coordination site was built using an imine formation reaction between the free amino groups of the MDA units and the 3-pyridinecarboxaldehyde (3-PA) complex precursors $[Pt(3\text{-}PA)_4](BF_4)_2$ ($\mathbf{Pt_{pyald}}$)[43] or *trans*-$[Ru(3\text{-}PA)_4Cl_2]$ ($\mathbf{Ru_{pyald}}$).[49] The synthesis of the non-symmetrically functionalized precursor **1** was achieved *via* amide coupling with nicotinic acid and *N*-Boc-4,4′-methylenedianiline in the presence of triethylamine (TEA) and *O*-(7-azabenzotriazol-1-yl)-*N*,*N*,*N*′,*N*′-tetramethyluronium hexafluorophosphate (HATU) under reflux. Removal of the protecting Boc group was achieved in a 1 : 5 trifluoroacetic acid : chloroform mixture to ultimately give pyridylamine derivative **2** (Scheme 1). Preparation of the cages $\mathbf{C^4_{Pt}}$ and $\mathbf{C^4_{Ru}}$ was accomplished through self-assembly between **2**, $[Pd(CH_3CN)_4](BF_4)_2$, and $\mathbf{Pt_{pyald}}$ or $\mathbf{Ru_{pyald}}$ in stoichiometric ratios of 4 : 1 : 1 at room temperature in dry DMSO, with a reaction time of *ca.* 24 h. The longer reaction time required relative to previously reported systems is likely due to the higher degree of flexibility of the linker in this case and the need to self-correct.[51] This helps to overcome the initial formation of the kinetically favored $[Pd_2(\mathbf{2})_4]^{4+}$ complex where ligand **2** is coordinated through the pyridyl and aniline N atoms, which

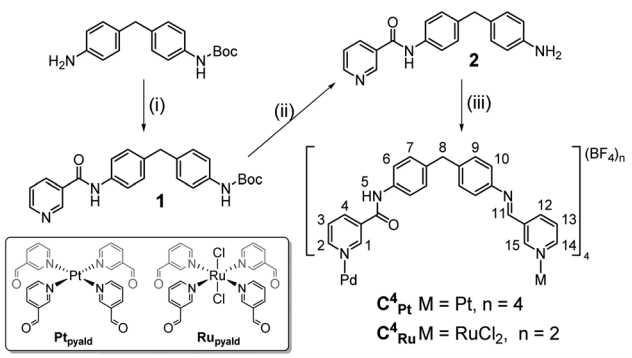

Scheme 1 Synthetic route to low-symmetry PdPt $\mathbf{C^4_{Pt}}$ and PdRu $\mathbf{C^4_{Ru}}$ cages. Reaction conditions: (i) nicotinic acid, HATU, TEA, CH_3CN, reflux, 16 h. (ii) TFA : $CHCl_3$ (1 : 5), 3 h. (iii) $[Pd(CH_3CN)_4](BF_4)_2$, $\mathbf{Pt_{pyald}}$ or $\mathbf{Ru_{pyald}}$, DMSO, 24 h.

has been previously observed by Chand and co-workers (Fig. S31–S33†).[32]

The formation of $\mathbf{C^4_{Pt}}$ and $\mathbf{C^4_{Ru}}$ was tracked by ^{1}H NMR spectroscopy, with each cage showing quantitative conversion after 24 h. The ^{1}H NMR spectra showed the steady diminution of the aldehyde and amine peaks from **2** and $\mathbf{Pt_{pyald}}$ or $\mathbf{Ru_{pyald}}$, respectively, with the appearance of imine signals at *ca.* δ 8.5–8.6 ppm. In addition, the pyridyl protons (H-1–H-4) shifted downfield upon coordination of the pyridyl-amide motifs to the Pd(II) center. Electrospray ionization-mass spectrometry (ESI-MS) data obtained showed a major peak for $[\mathbf{C^4_{Pt}}(-4BF_4)]^{4+}$ at m/z 467.6310 (m/z_{calc} 467.6311) with an isotopic pattern consistent with a PdPt system (Fig. S22†). For $\mathbf{C^4_{Ru}}$ a major peak at m/z 924.2015 was observed (m/z_{calc} 924.2011) corresponding to $[\mathbf{C^4_{Ru}}(-2BF_4)]^{2+}$ (Fig. S30†). ^{1}H DOSY NMR spectroscopy confirmed the resonances observed for $\mathbf{C^4_{Pt}}$ and $\mathbf{C^4_{Ru}}$ in each case corresponded to a single species, with diffusion coefficients of 1.16×10^{-10} and 2.78×10^{-10} m^2 s^{-1}, respectively. These values are consistent with larger assemblies compared to those of previously reported hetero- and homodimetallic cages.[43,44,46,48,50,51] $\mathbf{C^4_{Pt}}$ was isolated in high yield (92%) after the addition of ethyl acetate to the DMSO solution, whereas $\mathbf{C^4_{Ru}}$ could not be isolated in pure form by precipitation. However, NMR studies showed quantitative formation of this compound in solution and therefore solutions of $\mathbf{C^4_{Ru}}$ in DMSO or DMSO-d_6 were prepared as stock solutions for further studies. The molecular structure of $\mathbf{C^4_{Pt}}$ (Fig. 3) was determined by single crystal X-ray diffraction analysis. The structure featured three of the amide carbonyl moieties facing outwards, allowing the amide-NH groups to serve as H bond donors to encapsulated BF_4^- within the cavity, an orientation which is essential for binding of guests with H bond accepting properties (*vide infra*). Near the Pt center, three of the imine lone pairs are not available as H bond acceptors for guests due to their *exo* orientation. The structure is the largest heterodimetallic $PdPtL_4$ MSA reported so far with the Pd···Pt distance measuring at 15.48 Å, while $\mathbf{C^1_{Pt}}$–$\mathbf{C^3_{Pt}}$ (as well as $\mathbf{C^2_{Ru}}$ and $\mathbf{C^3_{Ru}}$) were in the range of 9.5–11.5 Å.[49] In contrast, the molecular structure of $\mathbf{C^4_{Ru}}$ (Fig. 3) features all four carbonyl oxygen atoms oriented towards the cavity and no classical H bond donors available for host–guest binding, while 'non-classic' short C–H···O bonds were observed to a co-crystallized guest DMSO molecule. In solution, the cages are more flexible, as shown by cross-peaks for the amide NH and imine CH protons to the neighboring endocyclic pyridyl protons in the NOESY spectra of both $\mathbf{C^4_{Pt}}$ and $\mathbf{C^4_{Ru}}$ (Fig. S18 and S26†). Although the Pd···M distances for $\mathbf{C^4_{Ru}}$ and $\mathbf{C^4_{Pt}}$, are similar (15.21 and 15.48 Å respectively) the presence of the *endo*-chlorido ligand in $\mathbf{C^4_{Ru}}$ reduces its cavity size considerably (Fig. 3). A significant difference was found in the packing for the two cages. They both stack linearly along the Pd···M axis, however, the intermolecular Pd···Ru distance is significantly shorter at 5.76 Å compared to the corresponding Pd···Pt spacing of 8.36 Å. This appears driven by electrostatic interactions between the *exo*-chlorido ligand of one $\mathbf{C^4_{Ru}}$ cage and the secondary coordination sphere of the Pd center of a neighboring molecule of $\mathbf{C^4_{Ru}}$ (Ru–Cl···Pd 3.34 Å).

Disassembly and reassembly reactions

Similar to the previously reported $Pd(\mu\text{-}L)_4Pt$ and $Pd(\mu\text{-}L)_4RuCl_2$ cage assemblies,[49] the larger cavity cages $\mathbf{C^4_{Pt}}$ and $\mathbf{C^4_{Ru}}$ showed selective disassembly at the palladium center upon addition of 4-dimethylaminopyridine (DMAP). Addition of DMAP to $\mathbf{C^4_{Pt}}$ or $\mathbf{C^4_{Ru}}$ in DMSO-d_6 resulted in decreasing intensities of the signals assigned to the heterodimetallic architectures in the ^{1}H NMR spectra. This was accompanied by the appearance of resonances attributed to the monometallic 'open-form' $[PtL_4]^{2+}$ and $[RuCl_2L_4]$ complexes, as well as a new set of peaks corresponding to $[Pd(DMAP)_4]^{2+}$ (Fig. 4).

Upon addition of *p*-toluenesulfonic acid (*p*-TsOH), the DMAP in $[Pd(DMAP)_4]^{2+}$ is protonated and the Pd ion re-coordinates to the accessible pyridyl nitrogen donors to reassemble the respective MSA. This process was slower than observed previously for $[PdPtL_4]^{4+}$ cages (1 day compared to several hours for

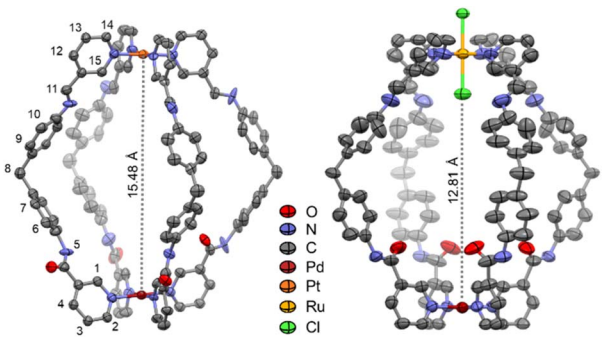

Fig. 3 Molecular structures of $\mathbf{C^4_{Pt}}$ (left) and $\mathbf{C^4_{Ru}}$ (right). The Pd···Pt and Pd···Cl intra-cage distances are highlighted by dashed lines. Hydrogen atoms, solvents and counteranions have been omitted for clarity. Due to the space group for $\mathbf{C^4_{Pt}}$, the representation is a combination of the Pt-imine and Pd-amide ends, superimposed at the bridging methylene groups (see Fig. S60† for clarity).

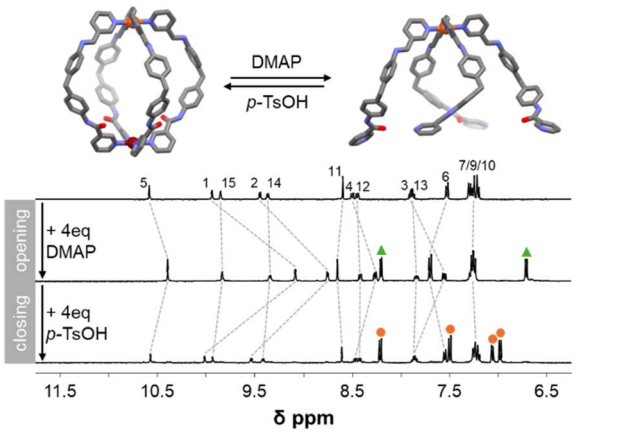

Fig. 4 Stacked ^{1}H NMR spectra (DMSO-d_6, 298 K, 400 MHz) of the disassembly of $\mathbf{C^4_{Pt}}$ upon addition of DMAP, and subsequent reassembly on addition of *p*-TsOH. Shifts in peaks are indicated with dashed lines. Spartan '24® MMFF models of the closed and open forms of $\mathbf{C^4_{Pt}}$ have been included for visualization. ▲ $[Pd(DMAP)_4](BF_4)_2$, ● (HDMAP)(TsO).

the smaller MSAs), most likely due to the greater length and higher flexibility of the bridging ligands.[43,46,49]

Host–guest chemistry

For the PdPt and PdRu MSAs $\mathbf{C^1_{Pt}}$–$\mathbf{C^3_{Pt}}$ and $\mathbf{C^1_{Ru}}$–$\mathbf{C^3_{Ru}}$, the anionic guests mesylate (**MsO**) and tosylate (**TsO**) were found to bind in the cavities of $\mathbf{C^3_{Pt}}$ and/or $\mathbf{C^3_{Ru}}$, and interactions with the neutral guests 5-fluorouracil and, to a minor extent, cisplatin were also observed.[49] The binding of guest molecules was influenced by the presence of H bond accepting and H bond donating groups, by coulombic and hydrophobic interactions, as well as steric constraints. In particular, the presence of the axial, *endo*-Cl ligand in $\mathbf{C^3_{Ru}}$ restricted the accessibility of the cage and partially compensated for the positive charge at the Ru center.

With the design of $\mathbf{C^4_{Pt}}$ and $\mathbf{C^4_{Ru}}$, it was anticipated that the steric constraints associated with guest binding would be relaxed and this would allow for easier access of guests into the cavities. Therefore, $\mathbf{C^4_{Pt}}$ and $\mathbf{C^4_{Ru}}$ were studied for their ability to interact with the **MsO** ($CH_3SO_3^-$) and **TsO** ($C_7H_7SO_3^-$) mono-anions as well as the larger di-anion 1,5-naphthalene disulfonate (**NDS**; $C_{10}H_6S_2O_6^{2-}$) by ^{1}H NMR spectroscopy and host–guest modelling. Larger disulfonates have been found by others to bind into the cavities of Pd_2L_4 cages.[53–57] For the mono-anionic guests, the modelling studies suggested that two guests would fit into the cavities of $\mathbf{C^4_{Pt}}$ and $\mathbf{C^4_{Ru}}$, whereas for the larger di-anionic **NDS** a single molecule would fill the space (Fig. S63 and S64†). In contrast, it was found that **NDS** could not bind effectively in the cavity of $\mathbf{C^4_{Ru}}$ and the smaller $\mathbf{C^3_{Pt}}$ (Fig. S65†). The binding constants (Table 1) were calculated from the NMR studies using the stoichiometries inferred by the Spartan '24® docking models (ESI†).

Titrations of **MsO** into a solution of $\mathbf{C^4_{Pt}}$ in DMSO-d_6 monitored by ^{1}H NMR spectroscopy showed interactions both inside and outside of the cage (Fig. S36 and S37†). For the interior protons H-1 and H-15, a plateau in the change of chemical shifts was reached at [G] : [H] ratios of *ca.* 6, whereas the exterior protons H-2 and H-14 did not plateau up to a [G] : [H] ratio of *ca.* 10. For $\mathbf{C^4_{Ru}}$, only very minor shifts for the interior protons were observed (Fig. S46 and S47†), indicating the role the *endo*-chlorido ligand plays in blocking H-15 from forming H bonds to guest molecules. In general, the binding constants observed for $\mathbf{C^4_{Pt}}$ and $\mathbf{C^4_{Ru}}$ were very small in comparison to $\mathbf{C^3_{Ru}}$ and, in particular, to $\mathbf{C^3_{Pt}}$. The weaker binding may be due to a mismatch between cavity and guest size.[49] The larger **TsO** guest interacted with protons inside and outside the cavity of $\mathbf{C^4_{Pt}}$ without reaching a plateau within 10 eq. of guest added (Fig. S38 and S39†), while it mainly interacted with the *exo*-cavity proton H-2 of $\mathbf{C^4_{Ru}}$ (Fig. S48 and S49†). The binding constants were slightly larger for both MSAs than observed for **MsO** which may be explained by favorable hydrophobic interactions, as also seen between two molecules of **TsO** in the cavity of $\mathbf{C^4_{Pt}}$ in modelling studies (Fig. S64†). As for **MsO**, the interaction with $\mathbf{C^3_{Pt}}$ was significantly more pronounced than for $\mathbf{C^4_{Pt}}$ (Table 1). The much larger cavity of $\mathbf{C^4_{Pt}}$ may not favor the encapsulation of **MsO** and **TsO**. The *endo*-chlorido ligand of the $RuCl_2$ motif of $\mathbf{C^4_{Ru}}$ reduces the cavity size compared to $\mathbf{C^4_{Pt}}$ and this is reflected by the smaller binding constant observed for **TsO**.

Significant shifts of signals in the ^{1}H NMR spectra were observed when titrating **NDS** into solutions of $\mathbf{C^4_{Pt}}$ (*e.g.*, H-15 shifted by *ca.* 0.4 ppm downfield, the amide proton H-5 by 0.1 ppm upfield), which can be explained by a combination of the sulfonate groups being excellent H bond acceptors, and also having a doubly negative charge compared to the single negative charges of **MsO** and **TsO**. The binding constant K obtained for **NDS** encapsulation by $\mathbf{C^4_{Pt}}$ was overall the highest at $> 10^5$ M^{-1} and demonstrates selectivity for this type of guest (Fig. 5). The binding of **NDS** in the cavity of $\mathbf{C^4_{Pt}}$ is likely driven by a combination of coulombic interactions of the sulfonate groups with both Pd(II) and Pt(II) metal centers as well as H bonding to the *endo*-α-pyridyl protons H-1 and H-15, similar to the interactions observed for quinones and other guests with related structures in previously reported homometallic MSAs.[17,43] These interactions result in a pseudo-chelate effect where the guest interacts with both "ends" of the cage cavity. Binding of **NDS** to $\mathbf{C^4_{Ru}}$ was observed to be much weaker (K = 1053 ± 168 M^{-1}) which reflects the effective blockage of the imine proton H-15 by the *endo* chlorido ligand (with loss of the chelate effect), the reduced effective charge at the Ru center and

Table 1 Binding constants K or K_1 observed for the MSAs C^4_{Pt} and C^4_{Ru} with MsO, TsO and NDS as guests as compared to C^1_{Pt}–C^3_{Pt} and C^1_{Ru}–C^3_{Ru} [49]

	Binding constants M^{-1}		
MSA	MsO	TsO	NDS
$\mathbf{C^1_{Ru}}$	75 ± 2	297 ± 66	—
$\mathbf{C^2_{Pt}}$	279 ± 11	237 ± 13	—
$\mathbf{C^2_{Ru}}$	209 ± 4	189 ± 7	—
$\mathbf{C^3_{Pt}}$	(1.30 ± 0.18) × 10^4	(3.50 ± 1.48) × 10^4	—
$\mathbf{C^3_{Ru}}$	314 ± 5	93 ± 3	—
$\mathbf{C^4_{Pt}}$	453 ± 5	581 ± 10	> 10^5
$\mathbf{C^4_{Ru}}$	283 ± 32	370 ± 44	1053 ± 168

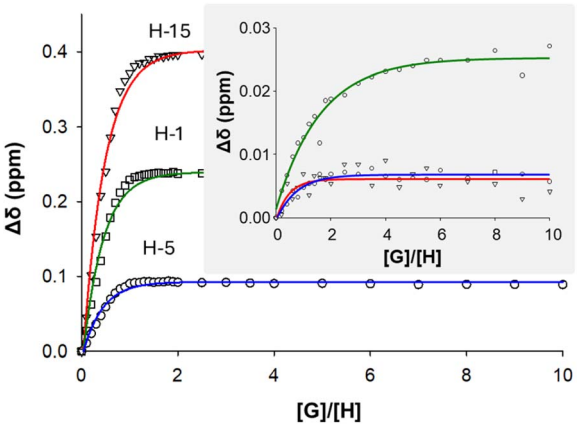

Fig. 5 Absolute changes in chemical shifts of H-1, H-5, and H-15 in the ^{1}H NMR spectra of C^4_{Pt} and C^4_{Ru} (inset) upon titration with up to 10 eq. NDS.

steric constraints, which consequently places the opposite sulfonate moiety into a non-ideal position or orientation for effective hydrogen bonding to protons H-1 and H-5 (Fig. S65†).

The interactions observed by NMR spectroscopy were supported by X-ray diffraction analysis of a crystal in which $\mathbf{C^4_{Pt}}$ was found to have encapsulated **NDS** ($\mathbf{C^4_{Pt}}\subset$**NDS**; Fig. 6). Each flexible arm adopted a unique orientation in space, as also seen in the molecular structure of $\mathbf{C^4_{Pt}}$, to allow for the accommodation of a single **NDS** molecule in the cavity. The sulfonate motifs form hydrogen bonds to two of the amide groups and two of the α-pyridyl protons at the Pd end of $\mathbf{C^4_{Pt}}$. At the Pt center, the second sulfonate motif formed H bonds to the *endo*-facing α-pyridyl protons. Host–guest complex formation was supported by coulombic interactions of the sulfonate groups of **NDS** with both the Pd and Pt centers, as seen for 1,8-naphthalimide sulfonates in Pd_2L_4 cages.[56] However, the observed solid state structure is a snapshot of one possible host–guest conformation, and the solution NMR data is consistent with dynamic interconversion between different conformations (Fig. S40†).

Investigation of the host guest properties of $\mathbf{C^4_{Pt}}$ and $\mathbf{C^4_{Ru}}$ conducted by ESI-MS confirmed the NMR spectroscopic data. Mass spectra of 1 : 1 mixtures of $\mathbf{C^4_{Pt}}$ and **MsO**, **TsO** or **NDS** gave peaks at *m*/*z* 655.1681, 680.5120, and 1079.2435 which were assigned to $[\mathbf{C^4_{Pt}}(-4BF_4)$ + **MsO**$]^{3+}$, $[\mathbf{C^4_{Pt}}(-4BF_4)$ + **TsO**$]^{,3+}$, and $[\mathbf{C^4_{Pt}}(-4BF_4)$ + **NDS**$]^{2+}$, respectively (Fig. 7 and S42–S44†), demonstrating interactions between the host and guest molecules. In competitive studies with 1 : 1 : 1 : 1 mixture of the anionic guests and $\mathbf{C^4_{Pt}}$, the stronger binding of **NDS** to $\mathbf{C^4_{Pt}}$ was evidenced by the appearance of only the $\mathbf{C^4_{Pt}}\subset$**NDS** peak, with no evidence of peaks corresponding to the $\mathbf{C^4_{Pt}}$, $\mathbf{C^4_{Pt}}\subset$**MsO**, or $\mathbf{C^4_{Pt}}\subset$**TsO** species (Fig. 7 and S45†). This may be likened to properties similar to the chelate effect found for multidentate ligands in metal complexes. Furthermore, the lower binding

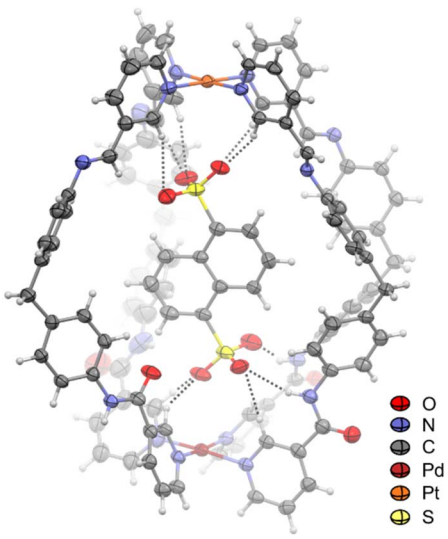

Fig. 6 Molecular structure of $\mathbf{C^4_{Pt}}\subset$**NDS** drawn at 50% probability level. Solvents and counteranions have been omitted for clarity. The dashed lines indicate H bonds between the NDS oxygen atoms and protons of $\mathbf{C^4_{Pt}}$.

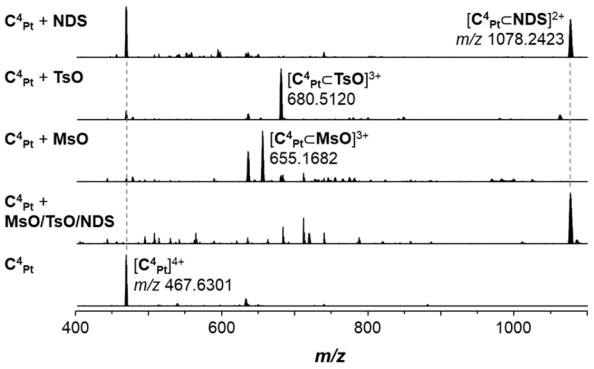

Fig. 7 Stacked mass spectra of $\mathbf{C^4_{Pt}}$, $\mathbf{C^4_{Pt}}$ incubated with **MsO**, **TsO**, or **NDS** (1 : 1) as well as with a mixture of guests (1 : 1 : 1 : 1).

constants observed for $\mathbf{C^4_{Ru}}\subset$**MsO**, $\mathbf{C^4_{Ru}}\subset$**TsO** and $\mathbf{C^4_{Ru}}\subset$**NDS** were consistent with the absence of host–guest complexes detected by ESI-MS.

Modelling (Spartan '24®, MMFF) of the host–guest chemistry of $\mathbf{C^4_{Pt}}$ and $\mathbf{C^4_{Ru}}$ with the neutral molecules cisplatin (**cis**), oxaliplatin (**ox**) and 5-fluorouracil (**5-FU**) within the cavities of $\mathbf{C^4_{Pt}}$ and $\mathbf{C^4_{Ru}}$ suggested 1 : 1, 1 : 2, and 1 : 3 adducts were possible (Fig. S66–S70†). Mixtures of these guests with $\mathbf{C^4_{Pt}}$ or $\mathbf{C^4_{Ru}}$ at molar ratios of 5 : 1 in DMSO-d_6 caused no shifts of proton resonances in the ^{1}H NMR spectra, most likely due to competition with DMSO for the binding site(s) within the cavities. However, qualitative guest-binding studies[17] of **cis**, **ox**, and **5-FU** with saturated solutions of $\mathbf{C^4_{Pt}}$ or $\mathbf{C^4_{Ru}}$ in CD_3CN or 10% DMSO/CD_3CN, respectively, could be carried out using ^{1}H NMR

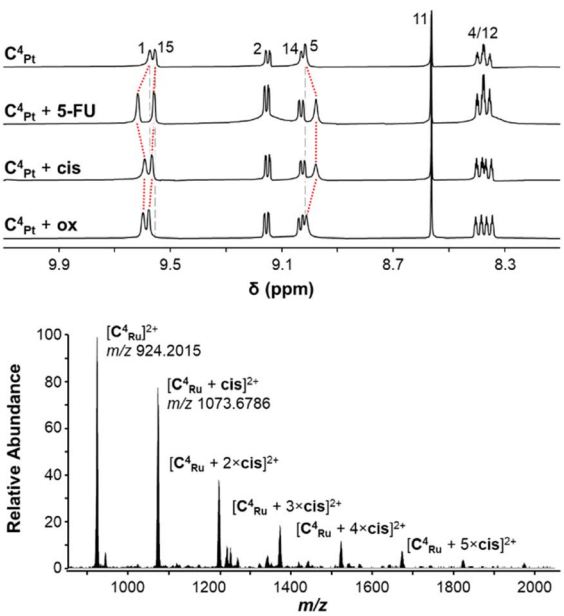

Fig. 8 (top) ^{1}H NMR spectra (CD_3CN, 298 K, 400 MHz) of $\mathbf{C^4_{Pt}}$ and mixtures of $\mathbf{C^4_{Pt}}$ with **5-FU**, **cis**, or **ox** (1 : 5). Shifts of *endo*-facing protons H-1, H-5, and H-15 are shown with dashed red lines. Vertical grey lines indicate the same chemical shift for the corresponding peak of $\mathbf{C^4_{Pt}}$ (top spectrum). (bottom) ESI-mass spectrum of a 1 : 5 mixture of $\mathbf{C^4_{Ru}}$ and **cis**.

spectroscopy (Fig. 8). The ^{1}H NMR spectra of $\mathbf{C^4_{Pt}}\subset$**cis** and $\mathbf{C^4_{Pt}}\subset$**5-FU** showed significant shifts of internally facing resonances (H-1, H-5 and H-15) while no effects on the externally facing protons H-2 and H-14 were observed (Fig. 8, S52 and S56†). Incubation with **ox** resulted in less pronounced changes but shifts of the *endo*-facing protons were still visible. These data point towards interactions of the drugs within the cage cavity, rather than externally around the Pd and Pt centers, as was seen with the anionic guests in addition to *endo*-bonding (*vide supra*). The overall changes in chemical shifts, however, were less pronounced than those of previously reported $MM'L_4$ MSAs with smaller cavities.[49] Based on the relative change in chemical shift of these internal protons, we can conclude that the guest species are bound closer to the Pd center, likely due to H bond formation between the carbonyl oxygen atoms and the platinum guests and the NH protons in the case of **5-FU**. Analogous studies with $\mathbf{C^4_{Ru}}$ revealed prominent shifts of the amide NH (H-5) and imine CH (H-11; Fig. S56†) with only minor shifts of *exo*-facing protons, also suggesting interaction within the cavity of $\mathbf{C^4_{Ru}}$. Broadening of peaks H-12, H-14, and H-15 was observed in CD_3CN (Fig. S56; † and to a lesser extent in DMSO-d_6), which may be explained at least in part by C–H···Cl interactions with the *exo*- and *endo*-chlorido ligands at the Ru center.

The mass spectra of 1 : 5 mixtures of $\mathbf{C^4_{Pt}}$ or $\mathbf{C^4_{Ru}}$ and **5-FU** indicated only weak interactions, with the **5-FU** adducts being detected at <5% abundances relative to the MSAs (Table S1, Fig. S53 and S57†). Mixtures of both MSAs with the platinum complexes however revealed for $\mathbf{C^4_{Pt}}$ host–guest complexes with up to two molecules of **cis** and 3 eq. of **ox** and even higher-level interaction with $\mathbf{C^4_{Ru}}$ with up to six molecules of **cis** or **ox** attached to the cage (Fig. 8, S54, S55, S58, S59 and Table S1†). Some of these interactions will occur on the outside of the cavity, facilitated by the chlorido ligands, as molecular modelling suggested a maximum of three molecules of **cis** or **ox** are able to be bound within $\mathbf{C^4_{Pt}}$ or $\mathbf{C^4_{Ru}}$ (Fig. S66–S70†). The higher number of adducts observed for $\mathbf{C^4_{Ru}}$ may be due to interactions between the *exo*-chlorido ligands and the Pt centers of the guests as found in the molecular structure of $\mathbf{C^4_{Ru}}$ (*vide supra*). The differences between **cis**/**ox** and **5-FU** to act as guest molecules can be explained by the H bond donating properties of the former. HCD (higher energy collisional dissociation) fragmentation of the isolated host–guest ions of $[\mathbf{C^4_{Pt}}]^{4+}$ and $[\mathbf{C^4_{Ru}}]^{4+}$ showed release of the guest molecules at NCE 10 (normalised collision energy) with the parent cage ions $[\mathbf{C^4_{Pt}}]^{4+}$ and $[\mathbf{C^4_{Ru}}]^{4+}$ remaining intact at *m*/*z* 467.6302 and *m*/*z* 924.2015, respectively (see Fig. S53–S55 and S57–S59†). The relative intensities of the host:guest ions *versus* the host ions at NCE 10 reflect differences in the gas phase stability of the inclusion complexes with the neutral guest molecules and decrease in the order **ox** > **cis** > **5-FU** for $\mathbf{C^4_{Pt}}$ and **5-FU** > **ox** > **cis** for $\mathbf{C^4_{Ru}}$.

Conclusions

Heterodimetallic $M(\mu\text{-L})_4M'$ MSAs based on non-symmetric bridging ligands have been shown to disassemble and reassemble upon the addition of external stimuli as well as host a variety of guest molecules in their cavities. We obtained the $Pd(\mu\text{-L})_4Pt$ $\mathbf{C^4_{Pt}}$ and $Pd(\mu\text{-L})_4RuCl_2$ $\mathbf{C^4_{Ru}}$ MSAs *via* subcomponent self-assembly using a 4,4′-methylenedianiline-based linker. This approach resulted in the largest $Pd(\mu\text{-L})_4M$ cages known so far. With inter-metal distances of 15.48 and 15.21 Å for $\mathbf{C^4_{Pt}}$ and $\mathbf{C^4_{Ru}}$, respectively, they are much larger than the closely related $\mathbf{C^1_{Pt}}$–$\mathbf{C^3_{Pt}}$ and $\mathbf{C^1_{Ru}}$–$\mathbf{C^3_{Ru}}$ MSAs. $\mathbf{C^4_{Pt}}$ and $\mathbf{C^4_{Ru}}$ underwent rapid selective opening at the Pd center upon addition of four eq. of DMAP to liberate palladium(II) as $[Pd(DMAP)_4]^{2+}$, however the kinetics of reassembly with addition of *p*-TsOH were much slower than found for the equivalent smaller cages, which can be explained by the increased flexibility and length of the bridging ligands. The sulfonate-containing guests **MsO** and **TsO** were bound only weakly in the cavities of $\mathbf{C^4_{Pt}}$ and $\mathbf{C^4_{Ru}}$. However, the 2^- charged guest **NDS** interacted strongly with $\mathbf{C^4_{Pt}}$ although the binding constant to $\mathbf{C^4_{Ru}}$ was 2 orders of magnitude lower. This lower binding constant can be attributed to the *endo*-chlorido ligand at the Ru center preventing H bonding to the internal α-pyridyl protons as well as reducing the coulombic interactions between the cage and the guest. Single crystal X-ray crystallographic studies demonstrated that the host–guest complex $\mathbf{C^4_{Pt}}\subset$**NDS** formed with one **NDS** guest occupying the cavity. The smaller MSAs $\mathbf{C^3_{Pt}}$ and $\mathbf{C^3_{Ru}}$ allowed effective discrimination between **MsO** and **TsO** based on size and coulombic interactions. However, these cages were too small to bind **NDS** effectively. The binding constants observed for $\mathbf{C^4_{Pt}}$ and $\mathbf{C^4_{Ru}}$ with **MsO** and **TsO** were significantly smaller when compared to $\mathbf{C^3_{Pt}}$ which we explain by a mismatch between cavity and guest size.

^{1}H NMR spectroscopy and ESI-MS also demonstrated binding with the neutral guests **cis**, **ox**, and **5-FU** within the cavity of both cages, with the number of guest molecules incorporated determined by the sizes and H bond donor properties of the guest molecules.

This study presents the second example of a $M(\mu\text{-L})_4M'$ cage with an octahedral metal center and demonstrates that the chlorido ligands coordinated to the Ru center have a larger role to play in tuning the host–guest interaction than anticipated from studies on smaller cages. Introduction of chlorido co-ligands expands the range of possible interactions that can occur between the host and guest molecules but also changes the overall charge of the cage and reduces direct accessibility to host metal centers, which are both important areas to further explore in the search for new applications of supramolecular architectures.

Data availability

The data supporting this article have been included as part of the ESI.†

Author contributions

Hayden B. Gearing: synthesis, binding studies, original draft; Monika Cziferszky: mass spectrometry studies; Tilo Söhnel: crystallography; L. James Wright: conceptualization, funding, writing – review and editing; James D. Crowley: supervision, conceptualization, funding, writing – review and editing; Christian G. Hartinger: supervision, conceptualization, funding, writing – review and editing.

Conflicts of interest

There are no conflicts to declare.

Acknowledgements

H. B. G. thanks the University of Auckland for a PhD scholarship. The work was supported by the Marsden Fund Council from Government funding (UOA1726), administered by the Royal Society of New Zealand. We are grateful to Dr Timothy Christopher and Dr Githal Arachchige for collecting the X-ray diffraction and mass spectrometry data.

References

1 S. J. Pike and P. J. Lusby, *Chem. Commun.*, 2010, **46**, 8338–8340.
2 A. Schmidt, A. Casini and F. E. Kühn, *Coord. Chem. Rev.*, 2014, **275**, 19–36.
3 N. B. Debata, D. Tripathy and H. S. Sahoo, *Coord. Chem. Rev.*, 2019, **387**, 273–298.
4 A. Pöthig and A. Casini, *Theranostics*, 2019, **9**, 3150–3169.
5 C. J. T. Cox, J. Hale, P. Molinska and J. E. M. Lewis, *Chem. Soc. Rev.*, 2024, **53**, 10380–10408.
6 V. Martí-Centelles, A. L. Lawrence and P. J. Lusby, *J. Am. Chem. Soc.*, 2018, **140**, 2862–2868.
7 R. L. Spicer, A. D. Stergiou, T. A. Young, F. Duarte, M. D. Symes and P. J. Lusby, *J. Am. Chem. Soc.*, 2020, **142**, 2134–2139.
8 X.-C. Zhou, L.-X. Wu, X.-Z. Wang, Y.-L. Lai, Y.-Y. Ge, J. Su, X.-P. Zhou and D. Li, *Inorg. Chem.*, 2022, **61**, 5196–5200.
9 J. E. M. Lewis, A. B. S. Elliott, C. J. McAdam, K. C. Gordon and J. D. Crowley, *Chem. Sci.*, 2014, **5**, 1833–1843.
10 A. B. S. Elliott, J. E. M. Lewis, H. van der Salm, C. J. McAdam, J. D. Crowley and K. C. Gordon, *Inorg. Chem.*, 2016, **55**, 3440–3447.
11 T. R. Cook, V. Vajpayee, M. H. Lee, P. J. Stang and K.-W. Chi, *Acc. Chem. Res.*, 2013, **46**, 2464–2474.
12 A. Casini, B. Woods and M. Wenzel, *Inorg. Chem.*, 2017, **56**, 14715–14729.
13 D. Preston, K. F. White, J. E. M. Lewis, R. A. S. Vasdev, B. F. Abrahams and J. D. Crowley, *Chem.–Eur. J.*, 2017, **23**, 10559–10567.
14 C. T. McTernan, J. A. Davies and J. R. Nitschke, *Chem. Rev.*, 2022, **122**, 10393–10437.
15 W. M. Bloch, S. Horiuchi, J. J. Holstein, C. Drechsler, A. Wuttke, W. Hiller, R. A. Mata and G. H. Clever, *Chem. Sci.*, 2023, **14**, 1524–1531.
16 D. A. McMorran and P. J. Steel, *Angew. Chem., Int. Ed. Engl.*, 1998, **37**, 3295–3297.
17 J. E. M. Lewis, E. L. Gavey, S. A. Cameron and J. D. Crowley, *Chem. Sci.*, 2012, **3**, 778–784.
18 S. Sharma, M. Sarkar and D. K. Chand, *Chem. Commun.*, 2023, **59**, 535–554.
19 N. Kishida, H. Sasafuchi, T. Sawada and M. Yoshizawa, *Chem. Sci.*, 2024, **15**, 13234–13239.
20 T. R. Cook and P. J. Stang, *Chem. Rev.*, 2015, **115**, 7001–7045.
21 X. Sun, D. W. Johnson, D. L. Caulder, K. N. Raymond and E. H. Wong, *J. Am. Chem. Soc.*, 2001, **123**, 2752–2763.
22 J. Yang, M. Bhadbhade, W. A. Donald, H. Iranmanesh, E. G. Moore, H. Yan and J. E. Beves, *Chem. Commun.*, 2015, **51**, 4465–4468.
23 C. Shen, A. D. W. Kennedy, W. A. Donald, A. M. Torres, W. S. Price and J. E. Beves, *Inorg. Chim. Acta*, 2017, **458**, 122–128.
24 D. Rota Martir, D. B. Cordes, A. M. Z. Slawin, D. Escudero, D. Jacquemin, S. L. Warriner and E. Zysman-Colman, *Chem. Commun.*, 2018, **54**, 6016–6019.
25 D. Rota Martir and E. Zysman-Colman, *Chem. Commun.*, 2019, **55**, 139–158.
26 M. Hardy, N. Struch, J. J. Holstein, G. Schnakenburg, N. Wagner, M. Engeser, J. Beck, G. H. Clever and A. Lützen, *Angew. Chem., Int. Ed.*, 2020, **59**, 3195–3200.
27 W. M. Bloch, Y. Abe, J. J. Holstein, C. M. Wandtke, B. Dittrich and G. H. Clever, *J. Am. Chem. Soc.*, 2016, **138**, 13750–13755.
28 W. M. Bloch, J. J. Holstein, W. Hiller and G. H. Clever, *Angew. Chem., Int. Ed. Engl.*, 2017, **56**, 8285–8289.
29 S. Sudan, R.-J. Li, S. M. Jansze, A. Platzek, R. Rudolf, G. H. Clever, F. Fadaei-Tirani, R. Scopelliti and K. Severin, *J. Am. Chem. Soc.*, 2021, **143**, 1773–1778.
30 D. Preston and J. D. Evans, *Angew. Chem., Int. Ed. Engl.*, 2023, **62**, e202314378.
31 E. Benchimol, I. Regeni, B. Zhang, M. Kabiri, J. J. Holstein and G. H. Clever, *J. Am. Chem. Soc.*, 2024, **146**, 6905–6911.
32 S. S. Mishra, S. V. K. Kompella, S. Krishnaswamy, S. Balasubramanian and D. K. Chand, *Inorg. Chem.*, 2020, **59**, 12884–12894.
33 P. Molinska, A. Tarzia, L. Male, K. E. Jelfs and J. E. M. Lewis, *Angew. Chem., Int. Ed. Engl.*, 2023, **62**, e202315451.
34 A. Tarzia, W. Shan, V. Posligua, C. Cox, L. Male, B. Egleston, R. Greenaway, K. Jelfs and J. E. M. Lewis, *Chem.–Eur. J.*, 2024, e202403336.
35 D. Preston, J. E. M. Lewis and J. D. Crowley, *J. Am. Chem. Soc.*, 2017, **139**, 2379–2386.
36 J. A. Findlay, K. M. Patil, M. G. Gardiner, H. I. MacDermott-Opeskin, M. L. O'Mara, P. E. Kruger and D. Preston, *Chem.–Asian J.*, 2022, **17**, e202200093.
37 J. E. M. Lewis, *Angew. Chem., Int. Ed.*, 2022, **61**, e202212392.
38 A. Platzek, S. Juber, C. Yurtseven, S. Hasegawa, L. Schneider, C. Drechsler, K. E. Ebbert, R. Rudolf, Q.-Q. Yan, J. J. Holstein, L. V. Schäfer and G. H. Clever, *Angew. Chem., Int. Ed.*, 2022, **61**, e202209305.
39 A. Kumar, S. Krishnaswamy and D. K. Chand, *Angew. Chem., Int. Ed.*, 2024, e202416332.
40 W. D. J. Tremlett, T. Söhnel, J. D. Crowley, L. J. Wright and C. G. Hartinger, *Inorg. Chem.*, 2023, **62**, 3616–3628.
41 S. Thoonen, S. E. Walker, S. Brandon, A. I. McKay, M. J. Paterson, J. D. Crowley, K. L. Tuck, D. R. Turner, *ChemRxiv*, 2025, DOI: 10.26434/chemrxiv-2024-lfgkf-v2.
42 H. B. Gearing, T. Söhnel, P. Young, L. Lisboa, L. J. Wright, J. D. Crowley and C. G. Hartinger, *Chem. Commun.*, 2024, **60**, 10950–10953.
43 L. S. Lisboa, J. A. Findlay, L. J. Wright, C. G. Hartinger and J. D. Crowley, *Angew. Chem., Int. Ed.*, 2020, **59**, 11101–11107.

44 L. S. Lisboa, M. Riisom, H. J. Dunne, D. Preston, S. M. F. Jamieson, L. J. Wright, C. G. Hartinger and J. D. Crowley, *Dalton Trans.*, 2022, **51**, 18438–18445.
45 L. Lisboa, D. Preston, J. McAdam, L. Wright, C. Hartinger and J. Crowley, *Angew. Chem., Int. Ed.*, 2022, **61**, e202201700.
46 A. C. Pearcy, L. S. Lisboa, D. Preston, N. B. Page, T. Lawrence, L. J. Wright, C. G. Hartinger and J. D. Crowley, *Chem. Sci.*, 2023, **14**, 8615–8623.
47 Z. T. Avery, M. G. Gardiner and D. Preston, *Angew. Chem., Int. Ed.*, 2024, e202418079.
48 L. Lisboa, D. Preston, J. McAdam, L. Wright, C. Hartinger and J. Crowley, *Angew. Chem.*, 2022, **61**, e202201700.
49 H. Gearing, T. Soehnel, P. G. Young, L. Lisboa, L. J. Wright, J. D. Crowley and C. Hartinger, *Chem. Commun.*, 2024, **60**, 10950–10953.
50 S. Bandi and D. K. Chand, *Chem.–Eur. J.*, 2016, **22**, 10330–10335.
51 Q. V. C. van Hilst, A. C. Pearcy, D. Preston, L. J. Wright, C. G. Hartinger, H. J. L. Brooks and J. D. Crowley, *Chem. Commun.*, 2024, **60**, 4302–4305.
52 *Spartan '24*, Wavefunction, Inc.
53 G. H. Clever, S. Tashiro and M. Shionoya, *Angew. Chem., Int. Ed.*, 2009, **48**, 7010–7012.
54 G. H. Clever, S. Tashiro and M. Shionoya, *J. Am. Chem. Soc.*, 2010, **132**, 9973–9975.
55 T. R. Schulte, J. J. Holstein and G. H. Clever, *Angew. Chem., Int. Ed.*, 2019, **58**, 5562–5566.
56 D. Preston, K. M. Patil, A. T. O'Neil, R. A. S. Vasdev, J. A. Kitchen and P. E. Kruger, *Inorg. Chem. Front.*, 2020, **7**, 2990–3001.
57 H. Lee, J. Tessarolo, D. Langbehn, A. Baksi, R. Herges and G. H. Clever, *J. Am. Chem. Soc.*, 2022, **144**, 3099–3105.